THE AMERICAN SOCIETY OF MECHANICAL ENGINEERS
345 E. 47th St., New York, N.Y. 10017

94-GT-31

COMPUTED ECCENTRICITY EFFECTS ON TURBINE RIM SEALS AT ENGINE CONDITIONS WITH A MAINSTREAM

Zhou Guo, David L. Rhode, and Fred M. Davis
Department of Mechanical Engineering
Turbomachinery Laboratory
Texas A&M University
College Station, Texas

ABSTRACT

A previously verified axisymmetric Navier-Stokes computer code was extended for three-dimensional computation of eccentric rim seals of almost any configuration. All compressibility and thermal/momentum interaction effects are completely included, and the temperature, pressure and Reynolds number of the mainstream, coolant stream and turbine wheel are fixed at actual engine conditions. Regardless of the seal eccentricity, both ingress and egress are found between θ = -30° and 100°, which encompasses the location of maximum radial clearance at θ = 0°. All other θ locations within the rim seal show only egress, as does the concentric basecase for all circumferential locations. Further, the maximum ingress occurs near θ = 30° for all eccentricities. This is found to produce a blade root/retainer temperature rise from the concentric case of 390 percent at 50 percent eccentricity and a 77 percent rise at 7.5 percent eccentricity. In addition, the nature of an increased eccentricity causing a decreased seal effectiveness is examined, along with the corresponding increase of cavity-averaged temperature.

NOMENCLATURE

a	Radial width of cavity inlet, constant
C_w	Volumetric flow rate parameter, $Q/(\upsilon R)$
dx(i)	Displacement along general orthogonal coordinate lines
e	Seal eccentricity (%)
E	Seal eccentric displacement (m)
GRZ	Gap recirculation zone
F	Force coefficient
h_i	Scale factor
H	Radial width of mainstream passage; stagnation enthaply
$H_i(j)$	Coordinate variation term
k	Turbulent kinetic energy
m_c	Mass flow rate of the cooling air
m_e	Mass egress across x-plane E-F [Fig. 1(a)]
m_i	Mass ingress across x-plane E-F [Fig. 1(a)]
$m_e/(m_c + \overline{m}_i)$	Sealing effectiveness
P	Static pressure
ΔP^*	Differential pressure, $[(P_T-P_1)/P_1]x10^3$
Q	Volumetric purge flow rate
R	Radius of disk
R_i	Radius of cooling air inlet slit into cavity
$Re_{x,m}$	Axial Reynolds number of mainstream, $(2UH)/\upsilon$
Re_ϕ	Rotational Reynolds number of disk, $(\Omega R^2)/\upsilon$
S	Axial width of cavity

Presented at the International Gas Turbine and Aeroengine Congress and Exposition
The Hague, Netherlands — June 13–16, 1994
This paper has been accepted for publication in the Transactions of the ASME
Discussion of it will be accepted at ASME Headquarters until September 30, 1994

S_c	Gap clearance between the rotor shroud and the stator shroud
T	Temperature
T^*	Normalized temperature, $(T-T_2)/(T_1-T_2)$
ΔT^*	Differential temperature, $2C_p(T_2-T_1)/(\Omega R)^2$
t	Radial thickness of shroud
U,V,W,	Mean velocities in x,r,θ directions
x,r,θ	Axial, radial, and tangential coordinates
x_i	Spatial coordinate in tensor notation
x^i	General orthogonal coordinate
Ω	Rotational velocity
ω_{whirl}	Shaft whirl frequency
μ	Absolute viscosity
υ	Kinematic viscosity
ρ	Fluid density, radial bipolar coordinate
ϵ	Turbulent energy dissipation rate
ϕ	Circumferential bipolar coordinate

Superscripts

*	Non-dimensionalized

Subscripts

1	Mainstream
2	Cooling purge flow

INTRODUCTION

The wheel spaces in gas turbine engines are typically sealed with a rim seal and are cooled by purge air bled from the compressor. In modern engines, the total coolant being bled approaches 20% of the throughflow. Clearly, this is a major penalty on the thermal efficiency and power output. Naturally a considerable amount of effort is being devoted toward using the bleed air in a more efficient manner. It is known that a considerable number of turbines are operated with the full awareness that hot gas ingestion into the wheelspace occurs in the downstream stsges. Therefore, designers are greatly interested in obtaining an enhanced understanding of the phenomena affecting this ingestion and heating of the turbine blade root retainer region of the wheel.

The present investigation builds on recent numerical developments (Ko and Rhode, 1991). For computstional economy reasons, that study considered the axisymmetric sub-problem af a generic rotor-stator cavity at actual engine temperature, pressure and Reynolds number of the cooling and main streams as well as the disk. This earlier work illuminated the presence and significance of a gap recirculation zone (GRZ) located slightly inward of a rim seal having a stator shroud. Specifically, it was shown how the GRZ is responsible for a large portion of the heat transport from the mainstream to the outer portion of the wheelspace. The presence of the GRZ in that study has been corroborated by measurements (Elovic, 1991) and by independent CFD computations revealed by Hendricks (1993) and by Ivey (1991). The present investigation provides an enhanced understanding of the effects of rim seal eccentricity on cavity and blade root/retainer thermal phenomena. Of particular interest is the effect of seal eccentricity on : (a) circumferential distribution of mainstream ingress and egress, (b) seal effectiveness, (c) cavity-averaged temperature and pressure, (d) location and temperature of rotor and stator hot spots and (e) circumferential distribution of blade root/retainer temperature.

Although numerous simple algebraic models exist for estimating $C_{w,min}$ without the interaction with the mainstream, there are apparently very few for estimating the ingress including mainstream effects. This situation is attributed to the complexity of: (a) the momentum/thermal flowfield and (b) the geometric layout of wheelspace cavities. Perhaps the first algebraic model for estimating ingress with a mainstream is that by Chew (1989). He proposed a model which combines the momentum-integral equations for cavity flows with a very simple seal model. Some of the basic seal mechanisms were not included, however, such that this model has uncertain applicability to various situations. Very recently Hamabe and Ishida (1992) assessed their algebraic ingress model by making gas concentration measurements in the wheelspace of a shrouded rotor-stator system with a nonaxisymmetric main flow. The asymmetry of the circumferential pressure distribution in the mainstream is the only 3-D effect on the turbine rim seal, and the rotor-stator cavity has been idealistically treated as being totally axisymmetric. It was found that the sealing effectiveness largely depends on the shape of the circumferential pressure distribution in the mainstream.

More sophisticated models using the Navier-Stokes equations have recently begun to appear in order to include all of the physical momentum and turbulence effects. Vaughan and Turner (1987) recently showed that, at least for certain conditions, a laminar 3-D solution gives a sinusoidslly varying ingress-egress cycle in the circumferential direction passing through a rim seal.

The most detailed numerical study of the three-dimensional rotor-stator cavity with external flow effects was conducted by Lowry and Keeton (1987). In their investigation, a CFD code with the two-equation (k-ϵ) turbulence model was used to compute the temperatures, pressures, and velocities in the High Pressure Fuel Turbopump aft-platform seal cavity of the Space Shuttle Main Engine for different boundsry conditions and geometries. The cavity temperature and pressure were approximately 1700°R (945°K) and 3600 psi (24.8 MPa), respectively. The 3-D cases computed were specified as:

(a) a prescribed asymmetric turbine exit pressure distribution based on pressure measurements (basecase), (b) an eccentric rim seal with a correspondingly eccentric coolant inlet and (c) a highly eccentric rim seal alone.

OBJECTIVE

The present objective is to obtain an enhanced understanding of the effects of rim seal eccentricity on the circumferential variation of : (a) ingress and egress rates, (b) cavity temperatures and pressures and (c) rim seal flow pattern. In addition, seal eccentricity effects on seal effectiveness and "hot spot" temperature as well as location are of interest. All compressibility and momentum/thermal effects at the mainstream interface will be accounted for using actual engine pressures, temperatures, and Reynolds numbers for the coolant and hot gas streams as well as the turbine wheel. Further, adiabatic walls are imposed in order to isolate ingress heating effects from wall heat convection effects.

NUMERICAL MODEL

Only the short axial space between an upstream stator vane and a downstream rotor blade, as well as the corresponding narrow axial segment of mainstream duct, has been modeled herein because the mainstream effect involved occurs only at the rim seal. The annular mainstream duct was radially shrunk in order to minimize the serious computing cost without affecting the solutions. Several computer solutions having a different mainstream radial extent were carefully compared in choosing a final domain which would minimize the number of grid points without affecting the solution. Figure 1(a) illustrates the idealized cavity showing the computational domain.

It was decided that approximating the mainstream passage as a straight annular duct is a very good approximation. This is due the fact that the effect of the diverging mainstream path is counterbalanced by the increasing boundary layer displacement thickness, which is caused by the high mainstream swirl velocity. This is particularly reasonable since : (a) only the short axial space between the stator vane and the rotor blade is of interest here and (b) an experienced turbine designer (Baskharone, 1990) was consulted concerning this decision.

An elliptic, axisymmetric Navier-Stokes computer code of the finite volume variety was recently extended to allow elliptic 3-D computations in most rim seal configurations at various seal eccentricities. The axisymmetric version had already given close agreement with measurements for a wide variety of test cases, including rotor-stator cavities (Ko and Rhode, 1991) as well as complex labyrinth seals. The current 3-D extension of the code has recently been tested, giving close agreement with rotordynamic measurements of a pump annular seal, a sample of which is discussed subsequently. A pressure-based method is used to solve the continuity, momentum and energy (stagnation enthalpy) equations as well as the turbulence model equations. Some of the basic approaches of the TEACH code of Gosman and Pun (1974) have been adopted. The primitive variables are solved on a system of three staggered grids using the SIMPLER algorithm of Patankar (1980). Leonard's (1979) QUICK convection differencing scheme is utilized for all convective terms in the momentum equations to reduce false diffusion. This differencing scheme was implemented in a special way by Rhode, et al. (1986) which promotes numerical stability.

Neglecting body forces, the steady-state continuity and momentum equations are

$$\frac{\partial(\rho U_i)}{\partial x_i} = 0$$

$$\frac{\partial(\rho U_i U_j)}{\partial x_i} = -\frac{\partial p}{\partial x_j} - \frac{\partial \tau_{ij}}{\partial x_i}$$

where ρ, U_i, and p are the time-averaged density, velocity, and pressure. The Reynolds stresses are determined by the higb Reynolds number k-ϵ turbulence model which is discussed later. Further, the stagnation enthalpy form of the energy equation

$$\frac{\partial (\rho U_i H)}{\partial x_i} - \frac{\partial}{\partial x_j}\left\{ \Gamma_H \frac{\partial H}{\partial x_j} \right\} = \frac{\partial}{\partial x_j}\left[U_i \tau_{ij} - \Gamma_H \frac{\partial}{\partial x_j}\left\{ \frac{V^2}{2} \right\} \right]$$

was included where:

$$\Gamma_H = \frac{\mu_{eff}}{Pr}$$

The static temperature was evaluated using:

$$T = \frac{H - \frac{1}{2}\left(U^2 + V^2 + W^2\right)}{C_p}$$

General Orthogonal Coordinates

The equations were transformed into relations involving general orthogonal coordinates using Pope's (1978) method. With his transformation procedure the equations retain their original form and simplicity as much as possible while being applicable to any orthogonal coordinate system, either numerically generated or algebraically specified.

Let x^i denote such a general orthogonal coordinate system. The scale factors h_i relate distances in this system to those in the Rectangular Cartesian system by

$$(ds)^2=(h_i dx^i)^2=[dx(i)]^2$$

where the scale factors h_i are excluded from the summation convention. Thus, dx(i) denotes the physical displacements along a coordinate line x^i in the general orthogonal coordinate system. The scale factors, which are excluded from the summation convention, are determined by

$$h_i^2=\sum_l \frac{\partial \bar{x}_l}{\partial x^i}\frac{\partial \bar{x}_l}{\partial x^i}$$

where $\bar{x}_l$ are the coordinates in the Cartesian coordinate system. Pope's divergence operator $\nabla(i)$ and coordinate variation term $H_i(j)$ needed to transform the transport equations into general orthogonal coordinates are

$$\nabla(i)=\frac{h_i}{|h|}\frac{\partial}{\partial x(i)}\frac{|h|}{h_i}$$

$$H_i(j)=\frac{1}{h_i h_j}\frac{\partial h_i}{\partial x_j}$$

Here h_i represents the scale factors and $|h|$ is the product of the scale factors. The transformed mass and momentum equations are

$$\nabla(i)[\rho U(i)]=0$$

and

$$\nabla(i)\,[\rho U(i)\,U(j)+\tau^*(ij)]=-\frac{\partial p^*}{\partial x(j)}$$

$$+H_i(j)\;[\rho U(i)U(i)+\tau^*(ii)]-H_j(i)[\rho U(i)U(j)+\tau^*(ij)]$$

The isotropic component of stress has been added to the pressure giving

$$p^* = p+\frac{2}{3}\rho k+\frac{2}{3}\mu_{eff}\,\nabla(i)\,U(i)$$

and τ^* involves the anisotropic stress as

$$\tau^*(ij) = -\mu_{eff}\left[\frac{\partial U(i)}{\partial x(j)}+\frac{\partial U(j)}{\partial x(i)}-U(i)\,H_i(j)-U(j)\,H_j(i)\right.$$

$$\left.+\;2\,U(l)\,H_i(l)\,\delta_{ij}\right]$$

The standard k-ϵ turbulence model was used. Concerning k-ϵ turbulence models, very recently Virr et al (1993) compared the wall function approach to a one-equation near-wall model for turbine disk cavities. They found that the wall function approach gave essentially the same results as integrating all the way to the wall if low rotational Reynolds numbers are avoided and if proper care is used in specifying the near wall mesh spacing. This overall conclusion was generally supported by the findings of Avva et al (1989), Avva et al (1990) and Williams et al (1991) who also compared wall functions with integration directly to the wall. The latter has the disadvantage for 3-D computations of substantially increasing the number of grid points where computational cost is already a serious concern. The rotational Reynolds number used herein is $7.62\text{x}10^6$, which is substantially more than sufficient to resolve the peak radial velocity along the disk surface. The values of y^+ in the important regions of large radius is approximately 100 while the values at small radius are near 200. This is exactly the range for which Virr, et al found best agreement with disk friction moment measurements.

The multi-scale k-ϵ model version recently developed and tested by Ko and Rhode (1990) has shown significant improvements for the more complicated turbulent flows such as the ones considered here. Although it does not require more grid points such as various 2-layer approaches, it has the disadvantage of requiring about 20 percent more CPU time and slightly more memory. Since the CPU time for the present solutions on our CRAY Y-MP computer was approximately 2.5 hours per computer solution using the standard k-ϵ model and wall function approach, it was decided to forego the multi-scale model for the moment. It is hoped that budgetary constraints will allow the multi-scale model in the near future. The execution memory requirement is currently 4.04 megawords.

Generating Eccentric Grids

In order to model geometries involving eccentricity without the complexity of numerically generating the grid, at least two coordinate systems must be used, one for eccentric regions and one for concentric regions. The bipolar coordinate system (Kamal, 1966) was employed in certain regions of the domain where geometric eccentricity occurs because: (a) its adjacent coordinate lines are eccentric with respect to each other and (b) it gives an orthogonal grid. This easily allows coordinate lines to fall on the desired eccentric surfaces of an eccentric rim seal for example. For the domain depicted in Fig. 1(a), cylindrical polar coordinates were utilized radially outward until the outer surface of the rotor shroud was reached. There a transition was made to bipolar coordinates, which extended radially outward across the rim seal radial clearance. At the inner surface of the stator shroud, a transition was made back to cylindrical coordinates which extended outward to the outer surface of the stator shroud. Then at the outer surface of the stator shroud a transition

was made to bipolar coordinates with displacement equal but opposite to that used in the rim seal radial clearance. Then a final transition was made to cylindrical coordinates which extended to the outer boundary of the domain.

This produced a stator shroud with an extremely small eccentric displacement of 0.95 mm (0.037 in) for the largest eccentricity case of 50%. This inverse approach to the geometric modeling of a rotor which is eccentric with respect to the stator housing was carefully scrutinized via examining the solution for each eccentricity case. It was very clear that the rim seal interaction of the hot and cold streams was entirely unaffected by the mainstream flow near the outer boundary of the domain due to the high mainstream velocity. Because this interaction is highly localized to the rim seal radial clearance region, as expected from earlier work, the same flow field is obtained for a radially displaced rotor as for a radially displaced stator. Subsequent velocity vector plots demonstrate the localized interaction.

The bipolar system of coordinates does not reduce to polar cylindrical coordinates at low eccentricity as does the modified bipolar system, and it requires a numerical procedure to determine the value of the constant "a" in order to obtain the desired geometry. However, the range of allowable eccentricities is much larger (0.1% to 99.9% of the clearance) compared to that for the modified bipolar system (0.0% to 1.0%). The former is limited only by the precision of the computer employed. Bipolar coordinates may be related to Cartesian coordinates by the following transformation

$$x = \frac{-\ a\sinh(\rho)}{\cosh(\rho)-\cos(\phi)}$$

$$y = \frac{a\sin(\phi)}{\cosh(\rho)-\cos(\phi)}$$

As for the modified bipolar system, ρ denotes the radius of a circle and ϕ denotes the circumferential position along that circle. The constant "a" is determined by a numerical search. The control volumes in an eccentric region are formed by the intersection of the bipolar coordinate lines as shown in Fig. 1(b). At the boundary of an eccentric region, the coordinates of the grid points are converted to the Cartesian system. This simplifies the conversion of the coordinates to the cylindrical system or another eccentric system in the adjoining region.

Comparison To 3-D Measurements

The strong circumferential effect in the rotordynamic measurements and predictions of Dietzen and Nordmann (1986) were selected to test the 3-D (i.e. circumferential) extension of the computer code. The earlier axisymmetric version of the model gave close agreement with measurements of rotor-stator cavities (Ko and Rhode, 1991) as well as labyrinth seals flowing liquids as well as gases

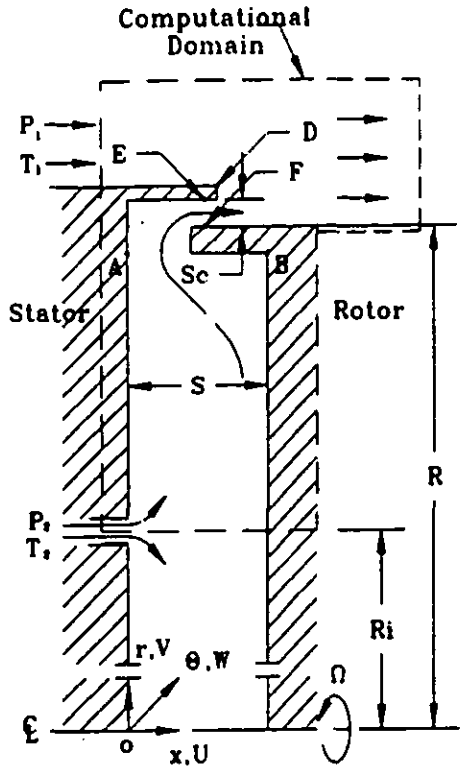

1(a) Configuration and computational domain

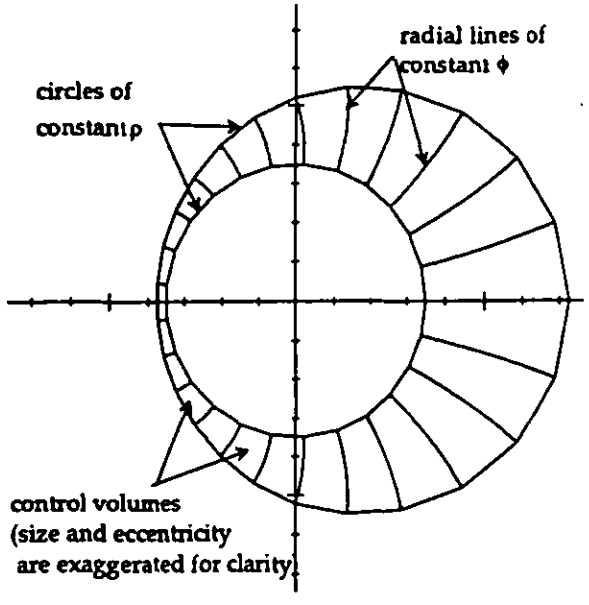

1(b) Extremely coarse bipolar coordinate mesh in an eccentric region of the grid

Fig. 1 (a) Configuration and computational domain and (b) extremely coarse bipolar coordinate mesh in an eccentric region of the grid

over an extremely wide range of Reynolds as well as Mach numbers. The case considered was a smooth annular seal flowing water at 30°C with the shaft whirling in a circular rotordynamic orbit at small eccentricity. This test case is most easily solved by removing the time variable from the problem. The preferred approach for accomplishing this is to use a reference frame which rotates and whirls with the shaft. Thus a "line of sight" viewed from this reference frame "sees", for example, the maximum clearance circumferential position at any instant of time. Thus the flow field relative to the observer has been converted to a steady flow in which the stator housing is rotating and whirling relative to the reference frame. The well known rotation-related extra source terms (Rhode, et al, 1993) were added to the radial and swirl momentum equations to account for the rotation of the reference frame. The relative motion relationship, which was derived to specify the velocity boundary conditions and initial guess relative to the current reference frame, is:

$$\overline{V} = \overline{v} + E\,\omega_{whirl} \sin\theta\, i_r + (E\cos\theta - r)\,\omega_{whirl}\, i_\theta$$

Here $\overline{v}$ is the velocity of any point relative to the seal outer housing. The current reference frame rotates at frequency ω_{whirl}, and its center whirls at tangential velocity $E\omega_{whirl}$ relative to the housing.

Grid independent computations of the measurements required 30 X 8 X 25 gridlines in the axial, radial and circumferential directions, respectively. To determine the stiffness and damping coefficients (defined below) for comparison with measurements, the fluid pressure force components in the direction of, and normal to, the shaft displacement were calculated from the CFD solution. This was done for five whirl speeds at each shaft speed. Then the force coefficients defined here were calculated by means of a least squares curve fit of the following relations

$$F_{Direct} = (K + d\omega_{whirl})\,E$$

$$F_{Indirect} = (-k + D\omega_{whirl})\,E$$

In these equations K and k are the direct and indirect stiffness whereas D and d are the direct and indirect damping coefficients, respectively. Further ω_{whirl} is the shaft whirl frequency and E is the shaft displacement. Figure 2 shows the comparison with measurements as well as a simple bulk model prediction which is believed to have been calibrated to similar measurements. The agreement is seen to be quite reasonable.

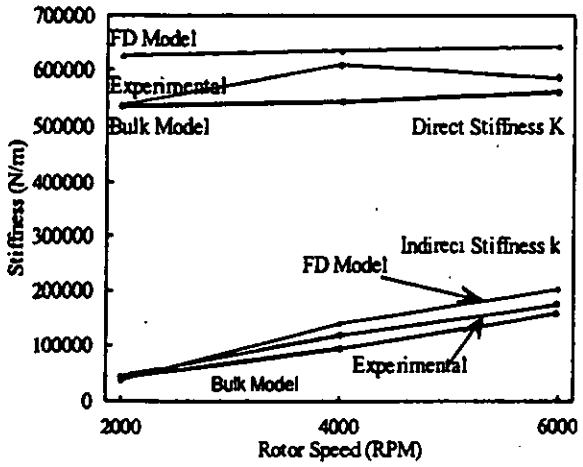

Fig. 2 Comparison of predictions with measurements of the rotordynamic stiffnesses from fluid pressure within an eccentric annular seal

RESULTS AND DISCUSSION

The complex momentum/thermal mixing details at the interface between the cavity and mainstream exert an important influence on blade root or retainer reliability. It has been known for some years that seal eccentricity has the potential of adversely affecting wheelspace heating due to increased hot gas ingress. An eccentric rotor naturally creates a circumferentially varying radial clearance for the type of rim seal configuration shown in Fig. 1(a). The eccentricity can be caused by the effects of rotordynamics, sideloads, or machining/assembly tolerances for example. Results from the idealized domain of Fig. 1(a) provide basic first-order insight into the little-known eccentricity effects on wheelspace heating by the mainstream.

Specifically, the first section gives a magnified view of the ingress/egress velocity vectors within the rim seal at four circumferential locations for 25 % eccentricity. The next section shows the effect of seal eccentricity on seal effectiveness as well as on cavity-averaged temperature and pressure. Moreover, the circumferential distribution of the ingress and egress mass flow are given for several eccentricities. The final section gives the circumferential variation of the temperature and pressure difference across the rim seal corresponding to each case of ingress/egress mass flow. In addition, the circumferential distribution of cavity local temperature and pressure is included.

An idealized turbine rim seal is shown in Figure 1(a), where the diameter of the rotor is different from that of the stator. A seal gap radial clearance of 1.9 mm and an overlap of the rotor shroud and the stator shroud of 2.0 mm were used following the work of Phadke and Owen (1988). Values of 7.5%, 25% and 50% were selected for the eccentricity of the seal. Other major dimensions of the generalized cavity considered are: (a) radius of the rotor R=0.3078m, (b) inlet radial width of the mainstream

passage H/R=0.026, (c) axial width of the cavity s/R=0.0612 (d) radial location of cavity inlet R_i/R=0.904 and (e) radial width of the cavity inlet a/R=0.00725. The cooling air enters the cavity axially through an annular slit in the stator at temperature T_2 and alao leaves axially through the radial gap between the rotor shroud and the stator shroud. The actual engine nominal conditions according to Ivey (1990) are: (a) axial Reynolds number in the main pass $Re_{z,m}=3.12\times10^5$, (b) rotational Reynolds number of the rotor $Re_\phi=7.62\times10^6$, (c) cooling flow rate $C_w=7200$, (d) differential pressure $\Delta P^*=-10$, (e) differential temperature $\Delta T^*=-4.6$, (f) swirl ratio at the main pass domain inlet W/U=tan(π/12) and (g) swirl ratio at the turbine cavity domain inlet W/U=0. The $Re_{z,m}$ above represents a mainstream axial velocity of 360m/sec which agrees with that of Ko and Rhode (1991) and Ko, Rhode and Guo (1993). The latter studies included an unnecessarily large radial portion of the mainstream which gave a correspondingly higher $Re_{z,m}$.

In order to focus on seal eccentricity effects alone, the inlet flow in the mainstream was approximated as uniform in the circumferential as well as the radial direction. This approximation was made for generality. It was based on discussions with two researchers employed by turbine companies, who indicated that the mainstream boundary layer at such high velocities would have a very small effect. The bipolar coordinate system was utilized in the eccentric region between the rotor shroud and the stator shroud as discussed earlier. A highly non-uniform grid of 44x44x25 in the x-, r- and θ-directions respectively was used for the computational domain shown in Fig. 1(a). The domain extends circumferentially from 0° to 360°. Comparison with solutions of finer non-uniform grids indicated that this grid gives the grid-independent circumferential distribution for ingress and egress flow rates.

Flow Distribution

The seal eccentricity of 25%, i.e. a 0.019 in (0.475 mm) displacement, was selected for analyzing the flow and thermal details of the seal/cavity domain. As expected, a large recirculation zone occurs in the wheelapace due to centrifugal forces, and a gap recirculation zone (GRZ) occurs downstream of the stator shroud for all θ planes. The GRZ is fairly consistent with the "impinging jet phenomenon" described by Owen and Rogers (1989) wherein a radial wall jet in the wheelspace flows outward along the rotor shroud and then turns counter-clockwise to flow inward along the stator.

Magnified views of the velocity vectors near the seal area at θ=0° and 86° are shown for this eccentricity case in Figs. 3(a) and 3(b). It is clearly seen how the incoming hot gas enters the seal along the outer surface of the rotor shroud. A portion of this incoming flow is turned clockwise almost 180 degrees by the pressure and centrifugal force fields near the seal. The θ-plane shown in Fig. 3(a) has the largest radial clearance and shows more inflow than

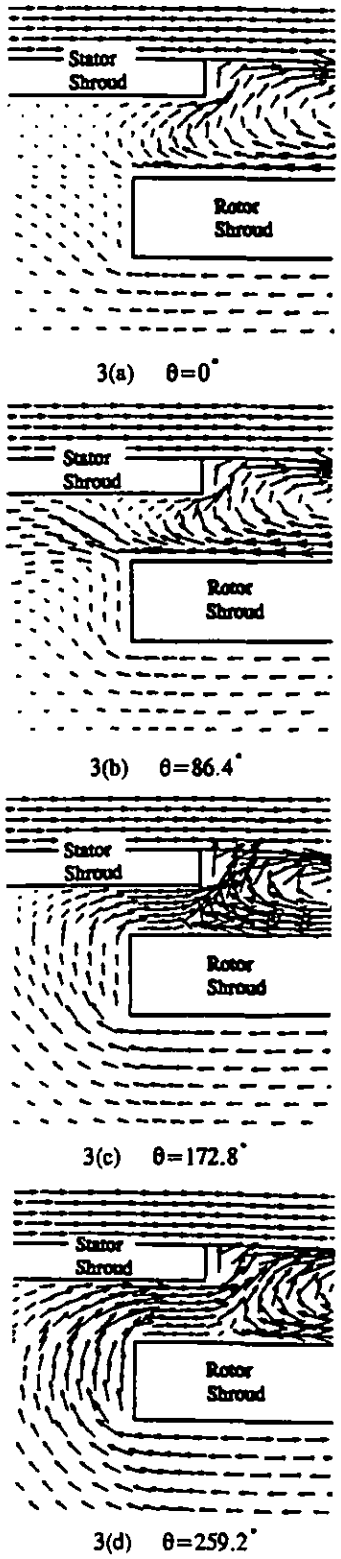

Fig. 3 Magnified view of velocity vectors near the gap region at 25% eccentricity for: (a) θ=0°, (b) θ=86.4°, (c) θ=172.8° and (d) θ=259.2° (the mainstream vectors have been scaled down 3.75 times for clarity)

outflow crossing axial station E-F (see Fig. 1(a)). For θ = 86°, Fig. 3(b) shows the slightly smaller radial clearance with a much greater portion of the incoming gas actually entering the cavity. In contrast, the coolant outflow rate is high enough to prevent ingress at θ=173° and 259° as shown in Figs. 3(c) and 3(d). The mainstream pressure is generally higher than that of the coolant fluid and naturally this is one contributing factor in favor of ingress. However, the concentric case computed herein gave no ingress and, as expected, gave an identical egress for all circumferential locations. For eccentric cases, the θ-location of large clearance [Fig. 3(a)] exhibits a significantly longer GRZ downstream of the stator shroud. This extra length allows a longer period of turbulent shear interaction with the very high velocity mainstream, which gives greater velocities within the GRZ.

Only for circumferential regions of high GRZ velocity is there sufficient momentum from right to left along the rotor shroud outer surface [Fig. 3(a)] for ingress to occur. The transit time required for a fluid particle to undergo shear from the mainstream, turn clockwise within the GRZ and flow from right to left (Fig. 3) along the rotor shroud explains why the greatest ingress (radially integrated across station E-F) occurs near θ=30° rather than θ=0°.

Rim Seal Performance

Figure 4 shows the seal effectiveness [$m_c/(m_c+\bar{m}_i)$] based on circumferentially averaged values of ingress, for all three eccentricities. Note that the coolant mass flow m_c has been kept constant and circumferentially uniform for all cases considered. As expected, as the eccentricity increases there is a considerable decrease in sealing effectiveness. The effects of this on cavity temperature and pressure is shown in Figure 5. Here the cavity-averaged (all axial, radial and circumferential locations) dimensionless temperature inside the cavity rises correspondingly for increasing eccentricity. This was clearly expected because more hot gas was known to ingest into the wheelspace for higher eccentricity. The average temperature at 50% eccentricity is about 16% higher than that for the concentric case. This is supported by the results of Lowry and Keeton (1987) who showed that, for the first two 3-D test cases, mentioned in an earlier section, the 3-D effect on the flow pattern in the cavity was very limited giving only a slight increase of the average cavity temperature. However, their third ease with a seal eccentricity of 75% indicated a significantly higher ingress. This gave an 80% increase in the temperature at the center of the cavity, compared with that of the basecase.

Figure 5 further shows a decreasing cavity-averaged pressure in the presence of an increasing eccentricity. This is attributed to the particular batance of pressure and centrifugal forces for this geometry at engine pressures, temperatures and Reynolds numbers. Interestingly, Lowry and Keeton found an increased cavity-averaged pressure for their eccentric CFD analysis of the High Pressure Fuel Pump rim seal cavity. However, this is not too surprising since their case had a drastically different cavity geometry and : (a) no stator shroud, (b) a mainstream pressure and temperature of 3600psi (24.8 MPa) and 1700°R (945°K) and (c) a rotor speed of 37,000 rpm.

The asymmetric distributions of the mass ingress and egress for eccentricities of 7.5%, 25%, and 50% are shown in Figs. 6(a), 6(b), and 6(c), respectively. Also shown here for reference is the distribution of seal radial clearance S_c. It is interesting that the ingress occurs for all three non-zero eccentricity cases considered, whereas none was found for zero eccentricity. Further, the magnitude of the ingress and the egress increases with eccentricity. As explained above, this is attributed primarily to increasing GRZ velocities at θ locations of larger seal radial clearance. Regardless of non-zero eccentricity, the maximum ingress occurs at θ = 30° and the maximum egress at about θ = 260°. As was mentioned previously, this ingress-egress cycle of the flow through the seal has a phase shift with respect to the S_c cycle because the swirl velocity convects the ingress in the circumferential direction.

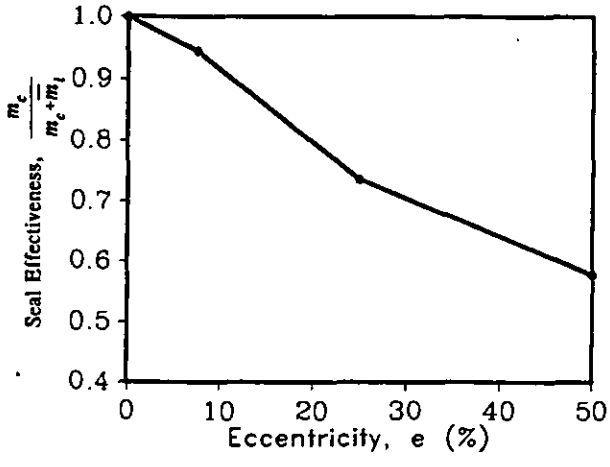

Fig. 4 Effect of eccentricity on the sealing effectiveness

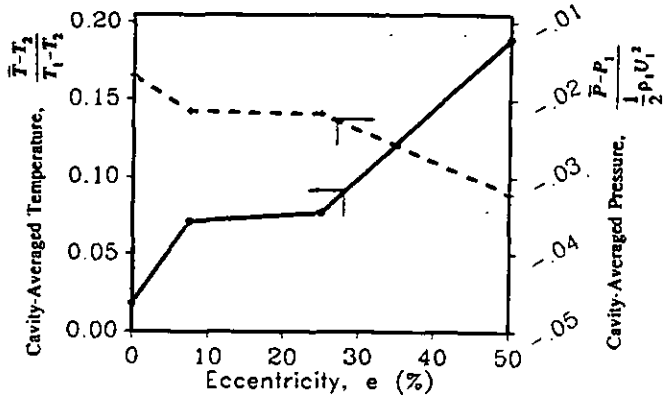

Fig. 5 Variation of the cavity-averaged temperature and pressure with eccentricity

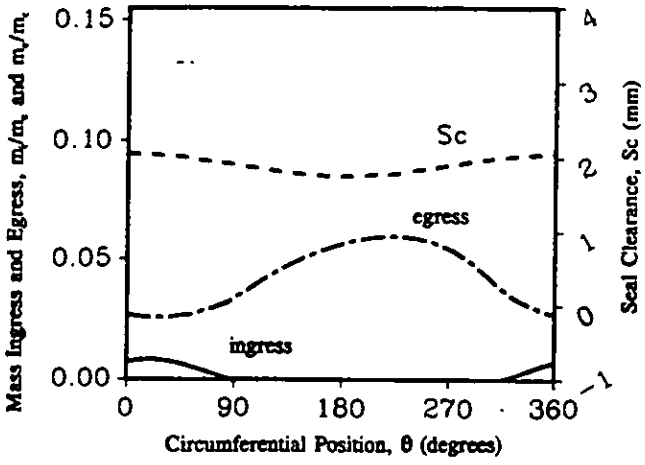

6(a) 7.5% eccentricity

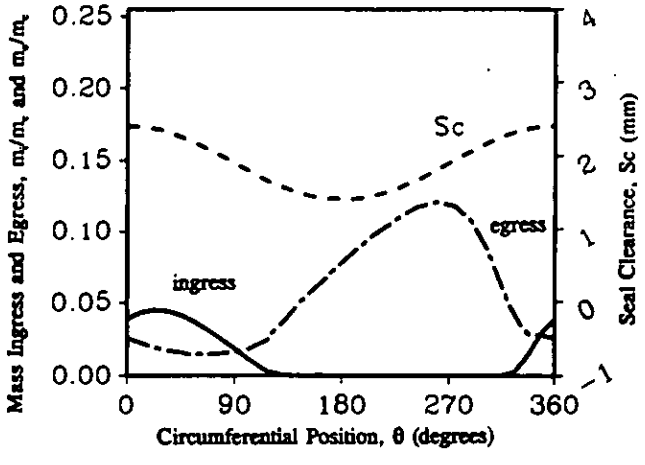

6(b) 25% eccentricity

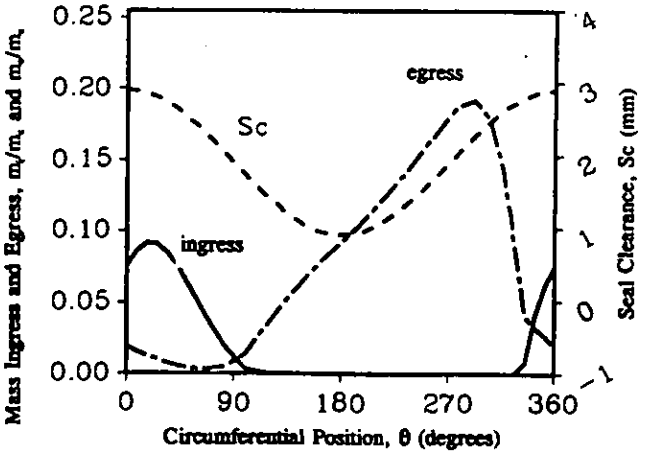

6(c) 50% eccentricity

Fig. 6 Circumferential variation of the mass ingress and mass egress as well as seal clearance for: (a) 7.5% eccentricity, (b) 25% eccentricity and (c) 50% eccentricity

Cavity Temperature and Pressure

Figures 7(a) through 7(c) show the circumferential temperature distribution at positions A and B (see Fig. 1(a)). Engine designers are especially interested in the temperature of location B because a primary cause of blade reliability concern is overheating of the blade root or retainer. As stated earlier, the ingested hot gases first contact the stator near location A, before mixing with the circulating flow in the cavity. The circumferential location with the highest temperature is shifted from θ = 30°, where most of the ingress occurs, to about 75° at position A and to about 180° at B because of a fluid particle's helical path between the seal and the particular location. Table 1 also gives the highest temperatures and their locations (hot spots) on the rotor as well as the stator for each case. These results are in good agreement with those in Figure 7. That is, as the eccentricity increases, the hot spot temperature increases considerably. It is also shown that positions A and B are close to the hot spots on the rotor and the stator, respectively. In addition, since the rotor is well protected by the shroud arrangement as well as by the coolant, the increase in temperature on the rotor with eccentricity is not severe like that on the stator.

Figures 8(a) through 8(c) show the circumferential pressure variation for the three eccentricities at positions A and D (see Fig. 1(a)). Since these figures give the circumferential distribution of pressure drop between A and D for the corresponding circumferential distribution of ingress in Figs. 6(a) through 6(c), one may develop or test a simple algebraic leakage model using these consistent figures. Further, the temperature difference between T_i and the cavity-averaged values from Fig. 7(a) through 7(c) may be utilized to develop or test a simple model of cavity heating.

The pressure in the mainstream is significantly higher than that inside the cavity for the concentric case. For eccentric cases the circumferential variation of pressure at locations A and D increases with eccentricity as expected. Here the pressure at position D is generally higher than that at A, except for a region between θ=190° and θ=280° for the 50% eccentricity case [Fig. 8(c)]. This circumferential region gives a higher cavity pressure in accordance with the ingress-egress circumferential distribution. Specifically, Fig. 6(c) shows the sharp peak of egress hear 280° which conserves mass across the rim seal by compensating for: (a) the small egress from θ=0° to θ=120° and (b) the total ingress. One would expect the pressure at A to be large in the high egress θ range to allow the large egress which occurs there.

For more global information, Figs. 9 and 10 show that the hot gases first contact the upper left corner of the cavity for 25% eccentricity. The strong cooling air jet recirculating in the cavity dilutes the high temperature of the ingested hot gases and cools the rotor. This is the reason why the greatest changes in temperature occur at the upper left corner region, and the average temperature of the cavity rises only 8% over that of the cooling air.

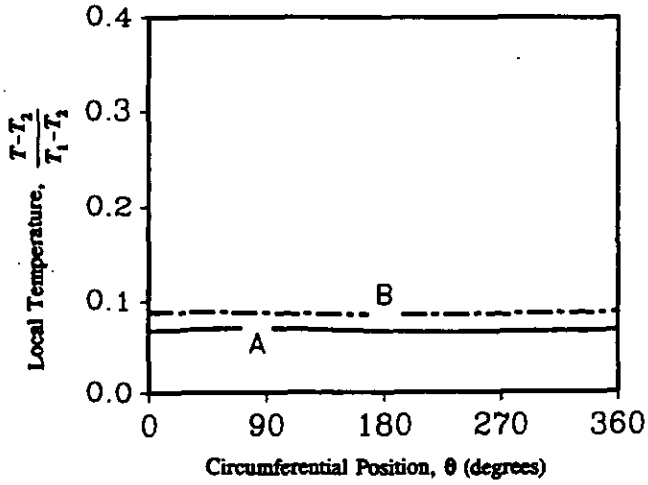

7(a) 7.5% eccentricity

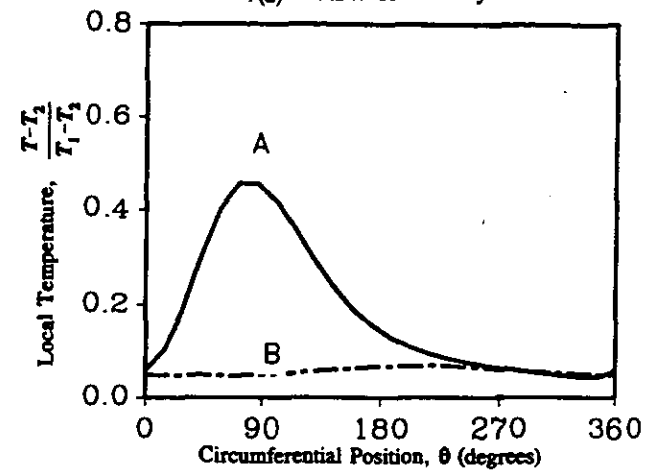

7(b) 25% eccentricity

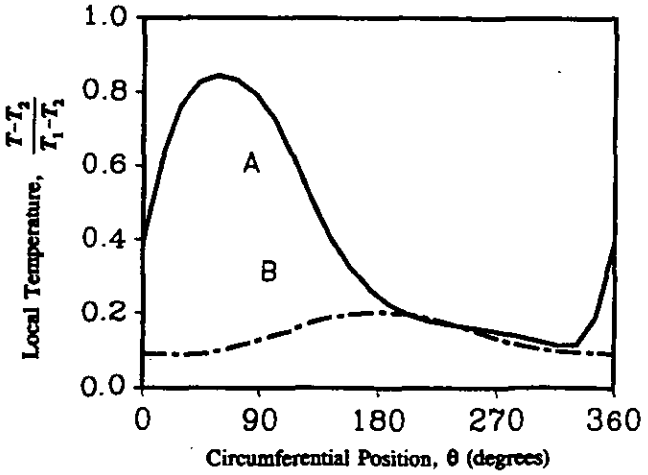

7(c) 50% eccentricity

Fig. 7 Circumferential variation of the dimensionless temperature at positions A and B (defined in Fig. 1(a)) for: (a) 7.5% eccentricity, (b) 25% eccentricity and (c) 50% eccentricity

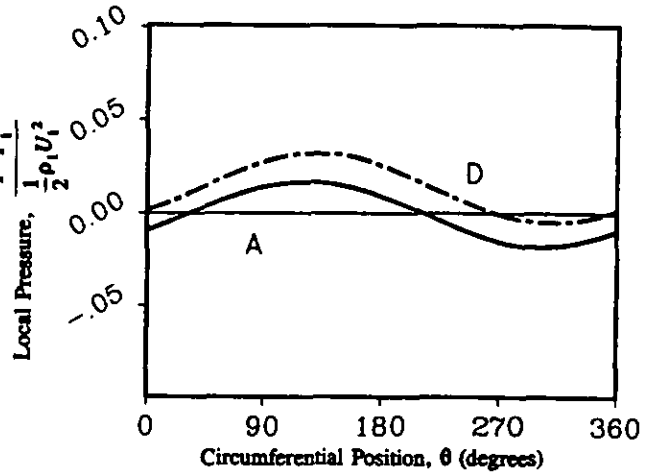

8(a) 7.5% eccentricity

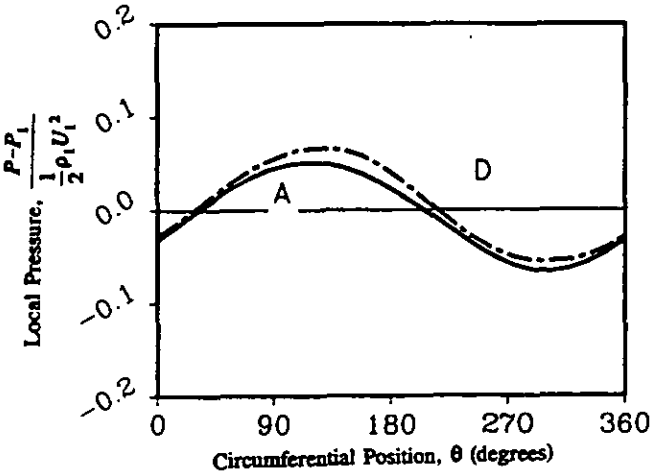

8(b) 25% eccentricity

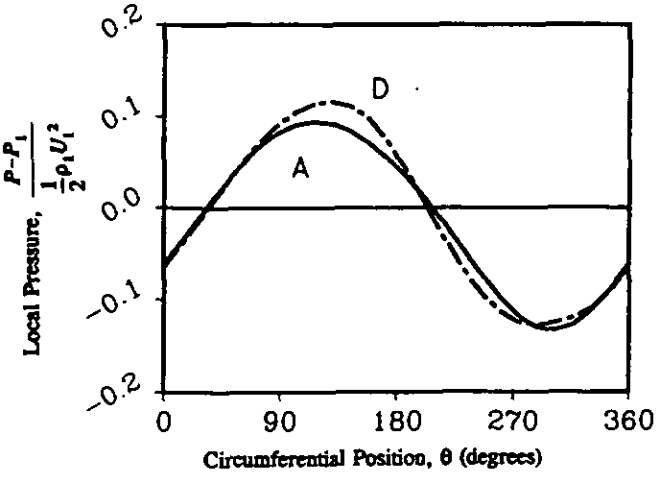

8(c) 50% eccentricity

Fig. 8 Circumferential variation of the dimensionless pressure at positions A and D (defined in Fig. 1(a)) for: (a) 7.5% eccentricity, (b) 25% eccentricity and (c) 50% eccentricity

Table 1 Hottest location and its temperature

	e (%)	$\frac{T_{max}-T_2}{T_1-T_2}$	r/R	θ (degrees)
Rotor	0	0.044	0.978	-
	7.5	0.078	0.978	14.4
	25	0.095	0.978	201.6
	50	0.216	0.906	129.6
Stator	0	0.018	0.94	-
	7.5	0.075	0.945	86.4
	25	0.552	0.993	71.3
	50	0.941	0.995	44.1

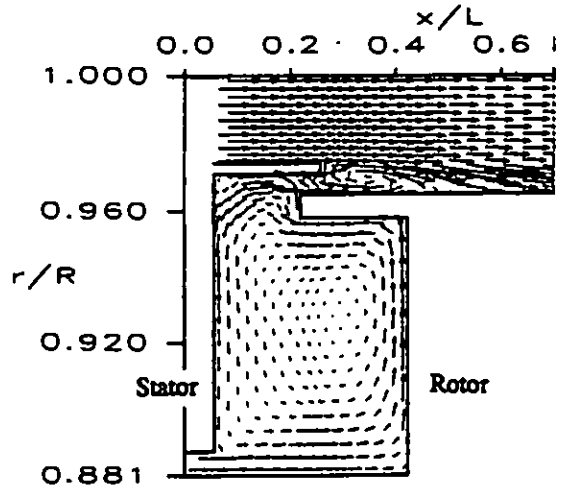

Fig. 9 Velocity vectors with 25% eccentricity for the θ=86.4° plane (mainstream vectors have been scaled down 3.75 times for clarity)

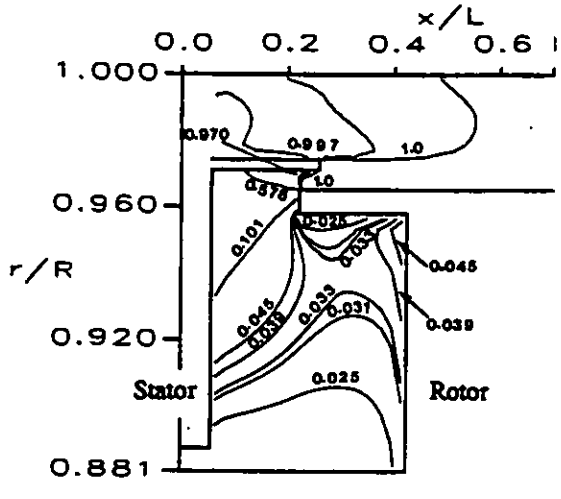

Fig. 10 Dimensionless isotherm contours with 25% eccentricity for the θ=86.4° plane

However, a significant ingestion to the inside of the cavity occurs at larger eccentricities causing the cavity-average temperature to increase by about 18% at 50% eccentricity.

CONCLUSION

A fully elliptic, three-dimensional Navier-Stokes model was developed from the axisymmetric version previously used for examining axisymmetric sub-problems such as the gap recirculation zone (GRZ) of rim seal cavities. The somewhat unexpected flow computations (Ko and Rhode, 1991) have been corroborated by measurements as explained by (Elovic, 1991) and by independent computations revealed by (Hendricks, 1993) and by Ivey (1991). The three-dimensional version of the code has a generalized capability of transitioning between any number and type of orthogonal coordinate systems in order to allow a wide range of eccentric seal configurations. The recent circumferential extension of this model was verified by comparison with rotordynamic measurements of a smooth, eccentric annular seal. The computer code was used to solve the 3-D problem of a rim seal interfacing with a mainstream at various eccentricities. Both the coolant and mainstream flow were fixed at nominal engine temperatures, pressures and Reynolds numbers; all walls were adiabatic so that temperature indicates ingress heating in addition to slight frictional heating in order to isolate this effect from the wall heat convection effect.

Specific findings include:

1. For non-zero eccentricities, both ingress and egress were found between θ= -30° and 100°, which encompasses the maximum radial clearance at θ = 0°. Other θ-planes showed only egress. This circumferential distribution was primarily attributed to higher GRZ velocities at θ locations of larger seal radial clearance.
2. Due to the circumferential convection effect resulting from the presence of swirl velocity, the maximum ingress was found at approximately θ = 30° for all non-zero eccentricities. This leads to the circumferential location of maximum rotor temperature, depending on eccentricity, in the wide range from θ = 15° to 202° and the location of maximum stator temperature from θ = 45° to 90°. Moreover, the ingress gives a blade root/retainer temperature rise from the concentric basecase (no ingress) of 390% at 50% eccentricity and a rise of 77% at 7.5% eccentricity.
3. The role of an increasing eccentricity producing a substantially decreasing seal effectiveness was examined, along with the corresponding substantial increase and decrease of cavity-averaged temperature and pressure, respectively.
4. Apparently cavity-averaged pressure can either decrease or increase over that of the concentric basecase depending on geometry and operating conditions.
5. The seal gap recirculation zone (GRZ) in the wake of the stator shroud was found to mix the mainstream and egress fluid so that the rim seal always encounters fluid at

essentially the mainstream temperature.
6. A significant once-per-revolution thermal cycle was found primarily for the e = 50% case, and the circumferential distribution of local temperature indicates the nature of this variation.
7. The difference between the circumferential distribution of the local pressure at locations A and D, which constitutes the distribution of local seal pressure drop corresponding to the distributions of ingress presented in Figs. 6(a) through 6(c), allows the development or testing of simple seal ingress prediction models at engine nominal temperatures, pressures and Reynolds number of the coolant flow, mainstream and disk.
8. The centrifugal force dominated the overall flow pattern as expected and prevented the ingress from directly contacting the rotor for eccentricities less than 25%.

ACKNOWLEDGMENTS

The authors are indebted to B. V. Johnson for his interest and assistance in identifying two important references. The authors are also grateful to the Supercomputer Center at the Texas A & M University for a grant of CRAY-YMP computer time.

REFERENCES

Avva, R. K., Ratcliff, M. L., and Leonard, A.D., (1989) "CFD Analysis of Rotating Disk Flows," in *Recent Advances and Applications in Computational Fluid Dynamics*, ASME Proceedings, FED-Vol. 103, pp. 99-105.

Avva, R., Smith, C. and Singhal, A., (1990), "Comparative Study of High and Low Reynolds Number Versions of k-ϵ Models," paper AIAA 90-0246.

Baskharone, E., (1990), private communication.

Chew, J. W., (1989), "A Theoretical Study of Ingress for Shrouded Rotating Disc Systems with Radial Outflow," paper ASME 89-GT-178.

Dietzen, F. J. and Nordmann, R., (1986), "Finite Difference Analysis for the Rotordynamic Coefficients of Turbulent Seals in Turbopumps," *Proceedings of Rotordynamic Instability Problems in High Performance Turbomachinery*, NASA CP-2443, Texas A&M University, pp. 269-284.

Elovic, E. (1991), General Electric Co., public discussion during technical sessions, International Gas Turbine and Aeroengine Congress, Orlando, Florida.

Gosman, A. D., and Pun, W. M., (1974), "Calculations of Recirculating Flows," Research Report, Report No. HTS/74/2, Department of Mechanical Engineering, Imperial College, London, England.

Hamabe, K. and Ishida, K., (1992), "Rim Seal Experiments and Analysis of a Rotor-Stator System with Nonaxisymmetric Main Flow," ASME Paper No. 92-GT-160.

Hendricks, R. C. (1993), NASA Lewis Research Center, public discussion during technical sessions, International Gas Turbine and Aeroengine Congress, Cincinnati, Ohio.

Ivey, P., (1990) personal communication.

Ivey, P., (1991), personal communication.

Ko, S. H. and Rhode, D. L., (1990), "Derivation and Testing of a New Multi-Scale k-ϵ Turbulence Model," AIAA-90-0243.

Ko, S. H. and Rhode, D. L., (1991), "Thermal Details In A Rotor-Stator Cavity At Engine Conditions With A Mainstream," *ASME Journal of Turbomachinery*, Vol. 114, pp. 446-453.

Ko, S. H., Rhode, D. L. and Guo, Z., (1993), "Computed Effects of Rim Seal Clearance and Cavity Width on Thermal Distributions," ASME paper 93-GT-419.

Kamal, M. M. (1966), "Separation in the Flow Between Eccentiric Rotating Cylinders," *ASME Journal of Basic Engineering*, Vol. 88, pp. 717-724.

Leonard, B. P., (1979), "A Stable and Accurate Convective Modelling Procedure Based on Quadratic Upstream Interpolation," *Computer Methods in Applied Mechanics and Engineering*, Vol. 19, pp. 59-98.

Lowry, S. A. and Keeton, L. W., (1987), "Space Shuttle Main Engine High Pressure Fuel Pump Aft Platform Seal Cavity Flow Analysis," NASA Technical Paper No. 2685.

Owen, J. M. and Rogers, R. H., (1989), *Flow and Heat Transfer in Rotating-Disc system: Vol. 1 Rotor-Stator Systems*, Research Studies Press, Taunton.

Patankar, S. V., (1980), *Numerical Heat Transfer and Fluid Flow*, McGraw-Hill, New York.

Phadke, U. P. and Owen, J. M., (1988), "Aerodynamic Aspects of the Sealing of Gas-Turbine Rotor-Stator Systems, Part 2: The Performance of Simple Seals in a Quasi-Axisymmetric External Flow," *Int. Journal of Heat and Fluid Flow*, Vol. 9, No. 2, pp. 106-112.

Pope, S. B., (1978), "The Calculation of Turbulent Recirculation Flows in General Orthogonal Coordinates," *Journal of Computational Physics*, Vol. 26, pp. 197-217.

Rhode, D. L., Demko, J. A., Traegner, U. K., Morrison,

G. L. and Sobolik, S. R., (1986), "Prediction of Incompressible Flow in Labyrinth Seals," Transactions of ASME, *Journal of Fluids Engineering*, Vol. 108, pp. 19-25.

Rhode, D. L., Hensel, S. J., and Guidry, M. J., (1992), "Labyrinth Seal Rotordynamic Force using a Three-Dimensional Navier-Stokes Code," Transaction of ASME, *Journal of Tribology*, Vol. 114, pp. 683-689.

Rhode, D. L., Hensel, S. J. and Guidry, M. J., (1993), "Three-Dimensional Computation of Rotordynamic Force Distributions in a Labyrinth Seal," *STLE Tribology Transactions*, Vol. 36, No. 3, pp. 461-469.

Sturgess, G. J., and Datta, P., (1988), "Calculation of Flow Development in Rotating Passages for Cooled Gas Turbine Blades," presented at the 33rd ASME International Gas Turbine and Aeroengine Congress and Exposition, Amsterdam.

Vaughan, C. M. and Turner, A. B., (1987), "Numerical Prediction of Axisymmetric Flow in a Rotor-Stator System with an External Mainstream Flow," *Proceedings 5th International Conference on Numerical Methods in Laminar and Turbulent Flows*, Swansea, United Kingdom.

Virr, G. P., Chew, J. W., and Coupland, J., (1993), "Application of Computational Fluid Dynamics to Turbine Disc Cavities," ASME paper No. 93-GT-89.

Williams, M., Chen, W. C., Bache, G., and Eastland, A., (1991), "An Analysis Methodology for Internal Swirling Flow Systems with a Rotating Wall," *ASME Journal of Turbomachinery*, Vol. 113, pp. 83-90.